Pergamon

Int. J. Heat Mass Transfer. Vol. 41, No. 11, pp. 1473–1484, 1998

Printed in Great Britain
0017-9310/98 $19.00+0.00

PII: S0017-9310(97)00220-2

A network thermodynamic analysis of the heat pipe

Z. J. ZUO and A. FAGHRI
Department of Mechanical Engineering, University of Connecticut, Storrs, CT 06269, U.S.A.

(*Received* 8 *November* 1996 *and in final form* 24 *July* 1997)

Abstract—This work provides a unique view into the physics behind the heat pipe operation which was considered a thermal network of various components. Transient heat pipe behavior was described by first-order, linear, ordinary differential equations. The working fluid undergoes a thermodynamic cycle which was analyzed by T–s diagrams. The heat pipe dimensions must be "thermally compatible" with the heat pipe materials to establish the thermodynamic cycle. This was illustrated by a dimensionless number proposed here for the first time. Validated by comparisons with previous experimental and numerical studies, the present thermodynamic theory may lead to simplified heat pipe design schemes. © 1998 Elsevier Science Ltd. All rights reserved.

INTRODUCTION

Over the past 30 years, extensive studies have been conducted in order to provide a thorough understanding of the heat pipe operation and appropriate design schemes for practical applications. As a result, numerous technical papers, focusing on various aspects off heat pipe operations have been published in journals and conference proceedings [1].

Previous experimental studies, concentrating on a variety of heat pipe aspects, have provided useful insights into heat pipe operations, set references for validation of theoretical models, and provided databases for design purposes. Additionally, many theoretical analyses incorporated empirical or semi-empirical correlations to simplify the models and the solution processes.

Most previous theoretical studies developed numerical methods to solve governing equations of the heat pipe operation. These numerical models ranged from lumped analysis to quasi-one-dimensional vapor flow to conjugated three-dimensional vapor flow and heat pipe wall heat conduction. A review of numerical models and solution methods for various heat pipe operations including steady-state, continuum transient and frozen start-up has been provided by Faghri [1]. Generally, previous theoretical models consisted of a set of highly nonlinear partial differential equations. To obtain solutions to these equations, numerical techniques such as finite-difference and finite-element methods must be incorporated, and significant programming efforts and computational time were required [2].

The complicated mathematical expressions and numerical schemes in previous studies were helpful, but sometimes may "mask" the real physics from a designer's point of view. For most practical applications, it is usually not desirable or necessary to get into such details. Therefore, a simple and understandable engineering model for the heat pipe analysis is attractive.

Vasiliev and Konev [3] considered the heat pipe a closed thermodynamic system and examined the effects of vapor super-heating and liquid subcooling. A heat pipe efficiency which indicates irreversibility losses in the system was defined based on the exergy balance of the heat pipe system. This was a pioneering work on thermodynamic analysis of the heat pipe operation. However, many aspects of the heat pipe operation such as the heat pipe transient, the working fluid circulation and the heat transfer limitations, were not discussed.

Faghri [1] summarized a "network" model of the steady-state heat pipe operation. The heat pipe was divided into nine components each with a specific thermal resistance. Estimation of the thermal resistance of each component was noted. The network model provided a simple way to calculate temperatures and heat fluxes in the heat pipe. However, the working fluid behavior and thus the working fluid related operating limitations could not be examined by this model. Additionally, only steady-state performance of the heat pipe was addressed.

Richter and Gottschlich [4] first proposed a thermodynamic cycle analogy to the heat pipe operation. The role of internal temperature/pressure differences was emphasized to be essential to the working fluid circulation. An interesting idea was proposed that the heat pipe operating temperature may be constrained by the temperature–pressure relation of the vapor phase working fluid. Although the authors' illustration of the liquid return process that the liquid temperature and entropy decrease on a T–s diagram was rather questionable, the thermodynamic cycle

NOMENCLATURE

A	cross-sectional area [m^2]
c_p	specific heat [$J\ kg^{-1}\ K^{-1}$]
D	diameter [m]
h	heat transfer coefficient [$W\ m^2\ K^{-1}$]
h'	specific enthalpy [$J\ kg^{-1}$]
h_{fg}	latent heat of vaporization [$J\ kg^{-1}$]
k	thermal conductivity [$W\ m\ K^{-1}$]
L	heat pipe length [m]
m	mass flow rate [$kg\ s^{-1}$]
P	pressure [Pa]
Q	heat transfer rate [W]
R	radius [m] or thermal resistance [$K\ W^{-1}$]
S	surface area [m^2]
s	specific entropy [$J\ kg\ K^{-1}$]
T	temperature [K or °C]
t	time [s]
W	work done during a process [J].

Greek symbols

α	thermal diffusivity [$m^2\ s^{-1}$] or angle defined in Fig. 3 [rad]
δ	wick thickness [m]
Θ	thermophysical properties group [m^2]
λ	material thickness of the heat conductor [m]
μ	viscosity [$N\ s\ m^{-2}$]
ξ, η, η'	constants defined in eqns (4)–(9)
ρ	density [$kg\ m^{-3}$]
Φ	geometric dimensions group [m^2]
φ	wick porosity
Ψ	dimensionless number defined in eqn (22).

Subscripts

∞	environment
A, B, C, D	working fluid states (Fig. 3)
a	adiabatic section
i,1 or i,2	end of heat conductor i
c	condenser
e	evaporator
eff	effective
HP	heat pipe
l	liquid
out	output
v	vapor
w	wick.

analogy did introduce a new and effective approach to heat pipe analysis.

There have been intense debate on whether the heat pipe operation can be modeled by a classical T–s diagram. One of the strongest opposing arguments was that the working fluid inside a heat pipe is seldom in an equilibrium state and consequently the working fluid state cannot be specified on a T–s diagram. However, the authors of the present paper would like to use an internal combustion engine as an example to validate the thermodynamic cycle approach.

In a typical internal combustion cylinder, the fuel is mixed with air to undergo a four-process cycle of intake, compression, power (combustion) and exhaust. Inside the cylinder is a mixture of air, fuel, water vapor, hydrocarbons and other substances resulting from the combustion. Each cycle lasts approximately 0.01 s for a 5000 rpm engine speed. Complete equilibrium is impossible to reach in such a rapid cycle containing so many chemical compounds. However, the internal combustion cycle has been successfully analyzed on T–s diagrams in numerous textbooks.

The focus of the present study is to provide a simplified engineering model of the heat pipe. Therefore, it is valid to use the thermodynamic cycle approach to analyze the working fluid which circulates in the heat pipe in a much slower pace than the internal combustion fluids.

In this paper, the "network" model was extended for transient heat pipe analysis. The heat pipe consists of a number of components with different thermal resistances and dynamic responses. Governing equations of the transient heat pipe behavior were simplified to a set of first-order, linear, ordinary differential equations. The working fluid circulation, one of the most important components, was viewed as a thermodynamic cycle. It was demonstrated that certain correlations between the heat pipe dimensions and the working fluid properties must be satisfied in order to establish the thermodynamic cycle. The analyses were compared with experimental and theoretical results available in the literature.

THEORETICAL ANALYSIS

A network model of the heat pipe system, consisting of a network of thermal resistance and a working fluid cycle, was first developed to analyze the heat pipe transients. Then the steady-state working fluid circulation and the related thermodynamic constraints were analyzed by T–s diagrams.

Network model

As illustrated in Fig. 1(a), the heat pipe operation consists of eight processes which can be classified into two categories: (1) pure heat transfer (or heat conduction) processes 1, 2, 4, 5, 7 and 8; and (2) heat and

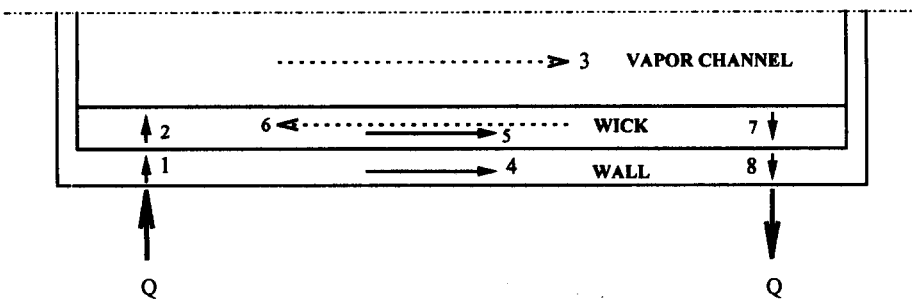

(a)

Process	Description
1	Radial heat conduction through the evaporator wall
2	Radial heat conduction through the evaporator liquid-wick
3	Vapor flow (heat convection)
4	Axial heat conduction through the adiabatic section wall
5	Axial heat conduction through the adiabatic section liquid-wick
6	Liquid flow (heat convection)
7	Radial heat conduction through the condenser liquid-wick
8	Radial heat conduction through the condenser wall

(b)

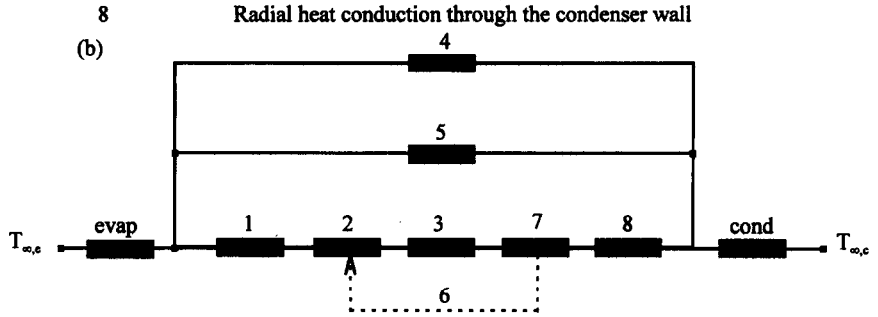

Fig. 1. A network system for the heat pipe operation. (a) A sketch of the heat pipe heat transfer. (b) A network analogy of the heat pipe heat transfer.

mass transfer (or heat convection) processes 3 and 6. Processes 3 and 6 form a working fluid circulation which plays an essential role in the heat pipe operation.

There is a thermal resistance associated with each of the eight heat transfer processes. Figure 1(b) illustrates a network of these processes as well as the convective heat transfer at the evaporator and condenser outer surfaces. Although the liquid return process 6 is extremely important to the working fluid circulation, it has little effect on the heat transfer (assuming negligible liquid–vapor interfacial heat exchange) and thus is illustrated by a dashed line.

A similar network has been presented by Faghri [1] and Dunn and Reay [5] for steady-state heat pipe analysis. Once the thermal resistance of each component (or process) is calculated, the heat pipe temperature at any location and heat flux in any process can be readily obtained.

It has been shown that vapor and wall transients have vastly different time scales [6, 7]. The authors of the present paper developed a numerical model including a transient wall heat conduction and a quasi-steady-state vapor flow. The results showed little difference compared to a fully transient model [8]. Furthermore, the vapor flow thermal resistance is considerably smaller than those of other processes. Therefore, the vapor flow can be neglected from the thermal network without causing significant errors.

The above argument implies that transient temperature behavior of the heat pipe mainly depends on the wall and wick heat conduction. It must be emphasized that although the working fluid presents little resistance to heat transfer, it does affect the heat pipe operation in another important way by maintaining a wetted evaporator surface so as to continue the heat transfer process. A much more detailed discussion of the effect of the working fluid is provided in the next section.

Since the heat pipe is viewed as a network system of heat conductors, system analysis theories can be used for transient heat pipe analysis. Figure 2(a) illustrates a one-dimensional heat conductor with a cross-sectional area of A_i and a thickness of λ_i. Two ends of the heat conductor are exposed to temperatures of $T_{i,1}$ and $T_{i,2}$, respectively. Assuming the temperature at the middle of the heat conductor is T_i, the following energy balance equations can be obtained:

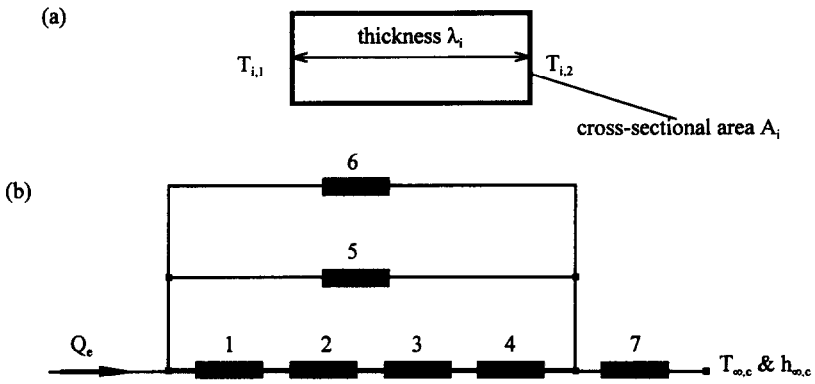

Component	Descriptions
Q_e	Evaporator heat input
1	Evaporator wall (radial direction)
2	Evaporator wick (radial direction)
3	Condenser wick (radial direction)
4	Condenser wall (radial direction)
5	Adiabatic wick (axial direction)
6	Adiabatic wall (axial direction)
7	Convective cooling condition (condenser outer surface)

Fig. 2. System analysis of the heat pipe operation. (a) A one-dimensional heat conductor. (b) A heat pipe network system.

$$\rho_i A_i \lambda_i c_{p,i} \frac{dT_i}{dt} = Q_{i,1} - Q_{i,2} \tag{1}$$

$$Q_{i,1} = k_i \frac{T_{i,1} - T_i}{\lambda_i/2} A_i, \quad Q_{i,2} = k_i \frac{T_i - T_{i,2}}{\lambda_i/2} A_i. \tag{2}$$

It should be noted that the input and output heat fluxes have been linearly approximated using Fourier's Law. If λ_i is very large (e.g. a thick wall or a long adiabatic section), this linear assumption may cause some errors. The component should then be divided into a series of heat conductors to ensure a smaller λ for each heat conductor. Rearranging eqns (1) and (2) gives

$$\frac{dT_i}{dt} = \frac{2\alpha_i}{\lambda_i^2}(T_{i,1} + T_{i,2} - 2T_i). \tag{3}$$

Equation (3) is the governing equation of each component (or process) in the heat pipe network as shown in Fig. 1(b), except for the vapor and liquid flows which have been assumed to have negligible effects on the heat pipe heat transfer. Figure 2(b) illustrates a heat pipe system consisting of six heat conductors in both series and parallel connections. The heat transfer rate into the system (Q_e), and the convective cooling conditions ($h_{\infty,c}$ and $T_{\infty,c}$) are given. If other heating and cooling conditions apply, corresponding changes must be made in the calculation.

Based on fundamental heat transfer principles, the system must obey the following two rules: (1) at any vertex, the summation of input heat flows equals the summation of output heat flows; and (2) the components (heat conductors) with a common vertex experience the same temperature at the corresponding ends.

Following the two rules and eqn (3), the governing equations of the heat pipe system are

$$\frac{dT_1}{dt} = \frac{2\alpha_1}{\lambda_1^2}[(\xi_{12} + \eta_1 - 2)T_1 + \xi_{21}T_2 + \eta_5 T_5 + \eta_6 T_6] + \frac{2\alpha_1}{\lambda_1^2} \frac{Q_e/2}{k_1 A_1/\lambda_1 + k_5 A_5/\lambda_5 + k_6 A_6/\lambda_6} \tag{4}$$

$$\frac{dT_2}{dt} = \frac{2\alpha_2}{\lambda_2^2}[\xi_{12}T_1 + (\xi_{21} + \xi_{23} - 2)T_2 + \xi_{32}T_3] \tag{5}$$

$$\frac{dT_3}{dt} = \frac{2\alpha_3}{\lambda_3^2}[\xi_{23}T_2 + (\xi_{32} + \xi_{34} - 2)T_3 + \xi_{43}T_4] \tag{6}$$

$$\frac{dT_4}{dt} = \frac{2\alpha_4}{\lambda_4^2}[\xi_{34}T_3 + (\xi_{43} + \eta_4 - 2)T_4 + \eta_5' T_5 + \eta_6' T_6] + \frac{2\alpha_4}{\lambda_4^2} \frac{h_{\infty,c} S_c T_{\infty,c}/2}{k_4 A_4/\lambda_4 + k_5 A_5/\lambda_5 + k_6 A_6/\lambda_6 + h_{\infty,c} S_c/2} \tag{7}$$

$$\frac{dT_5}{dt} = \frac{2\alpha_5}{\lambda_5^2}[\eta_1 T_1 + \eta_4' T_4 + (\eta_5 + \eta_5' - 2)T_5 + (\eta_6 + \eta_6')T_6] + \frac{2\alpha_5}{\lambda_5^2} \frac{Q_e/2}{k_1 A_1/\lambda_1 + k_5 A_5/\lambda_5 + k_6 A_6/\lambda_6}$$

$$+\frac{2\alpha_5}{\lambda_5^2}\frac{h_{\infty,c}S_cT_{\infty,c}/2}{k_4A_4/\lambda_4+k_5A_5/\lambda_5+k_6A_6/\lambda_6+h_{\infty,c}S_c/2} \quad (8)$$

$$\frac{dT_6}{dt}=\frac{2\alpha_6}{\lambda_6^2}[\eta_1T_1+\eta_4'T_4+(\eta_5+\eta_5')T_5$$

$$+(\eta_6+\eta_6'-2)T_6]+\frac{2\alpha_6}{\lambda_6^2}\frac{Q_e/2}{k_1A_1/\lambda_1+k_5A_5/\lambda_5+k_6A_6/\lambda_6}$$

$$+\frac{2\alpha_6}{\lambda_6^2}\frac{h_{\infty,c}S_cT_{\infty,c}/2}{k_4A_4/\lambda_4+k_5A_5/\lambda_5+k_6A_6/\lambda_6+h_{\infty,c}S_c/2} \quad (9)$$

where

$$\xi_{ij}=\frac{k_iA_i/\lambda_i}{k_iA_i/\lambda_i+k_jA_j/\lambda_j},$$

$$\eta_i=\frac{k_iA_i/\lambda_i}{k_1A_1/\lambda_1+k_5A_5/\lambda_5+k_6A_6/\lambda_6}$$

and

$$\eta_i'=\frac{k_iA_i/\lambda_i}{k_4A_4/\lambda_4+k_5A_5/\lambda_5+k_6A_6/\lambda_6+h_{\infty,c}S_c/2}.$$

Equations (4)–(9) are first-order, linear, ordinary differential equations which can be solved by fourth-order Runge–Kutta method. Once temperatures at various locations in the heat pipe are obtained, other parameters such as heat fluxes, temperature gradients and the heat pipe efficiency can be easily calculated. In the next section, temperature drops in the vapor and liquid working fluid, the primary interest of this paper, are calculated using this network model.

Working fluid circulation

The heat pipe working fluid functions as a thermal energy "carrier" which cycles between the evaporator and condenser. Since its transient response is almost spontaneous and its thermal resistance is negligible, the working fluid presents negligible effect on transient temperature distribution in the heat pipe. However, it is very important for the working fluid to continuously circulate in the heat pipe. Without the carrier (working fluid), the thermal energy can never reach the destination (condenser). If the carrier cannot successfully return to the evaporator, the next dispatch becomes impossible and the heat pipe operation discontinues.

The two-phase working fluid circulation is pumped by the internal pressure differences between the evaporator and condenser [4]. The working fluid circulation consists of four processes: (1) in the evaporator, the liquid absorbs heat and turns into vapor; (2) the vapor travels through the adiabatic section due to the pressure difference between the evaporator and condenser; (3) in the condenser, the vapor releases the latent heat and condenses into liquid; and (4) the liquid returns to the evaporator through the wick structure by the wick capillary force, a result of the pressure difference between the evaporator and condenser.

Figure 3 shows the four processes on a T–s diagram. The vapor phase working fluid at state B can be slightly superheated in some cases. Entropy increases during the vapor flow process B–C and the liquid flow process D–A due to irreversibility from friction in the fluid flows. The working fluid at state C can be saturated or slightly superheated depending on friction losses in the vapor flow. It was assumed that the condenser heat rejection process C–D occurs at a constant pressure. State D must be subcooled in order to obtain a stable heat pipe performance, which is discussed in more detail later in this section. The heat addition process A–B not only raises the internal energy level of the working fluid, but also provides the essential "regaining" of the working fluid pressure which is lost due to the vapor and liquid flow friction. The evaporator liquid–vapor interface is like a "vapor diode" which separates the lower-pressure liquid and the higher-pressure vapor. It is the thermal energy input (i.e. heat addition) that drives the working fluid across the liquid–vapor interface [1] and thus provides the "pumping power" for the working fluid circulation [4].

If the liquid in the condenser, state D, is not subcooled to an adequate level, the working fluid may enter a two-phase zone after traveling through the adiabatic section (state A). Substantial evaporation or vaporization in the wick structure in the adiabatic section results in less liquid returning to the evaporator, which may contribute to an unstable heat pipe operation.

Applying the conservation of energy to each process and neglecting potential and kinetic energy yields the following:

$$Q_{A\text{–}B}=m(h_B'-h_A') \quad (10)$$

$$m(h_C'-h_B')=W_{B\text{–}C}=\frac{m}{\rho_v}(P_{v,C}-P_{v,B}) \quad (11)$$

$$m(h_D'-h_C')=Q_{C\text{–}D} \quad (12)$$

$$m(h_A'-h_D')=W_{D\text{–}A}=\frac{m}{\rho_l}(P_{l,A}-P_{l,D}). \quad (13)$$

Equations (10)–(13) clearly indicate the energy conversion and transport during the four processes: (1) in process A–B, heat addition $Q_{A\text{–}B}$ raises the enthalpy (internal energy and pressure) of the working fluid from h_A' to h_B'; (2) in process B–C, a portion of the thermal energy possessed by the working fluid is converted into the pumping power to overcome the frictional work $W_{B\text{–}C}$ which is directly related to the vapor pressure difference; (3) in process C–D, the working fluid releases its thermal energy in the form of heat rejection; and (4) in process D–A, a portion of the thermal energy is converted into the pumping power to overcome the frictional work $W_{D\text{–}A}$ which is directly related to the liquid pressure difference. Heat exchange between the vapor and the liquid in processes

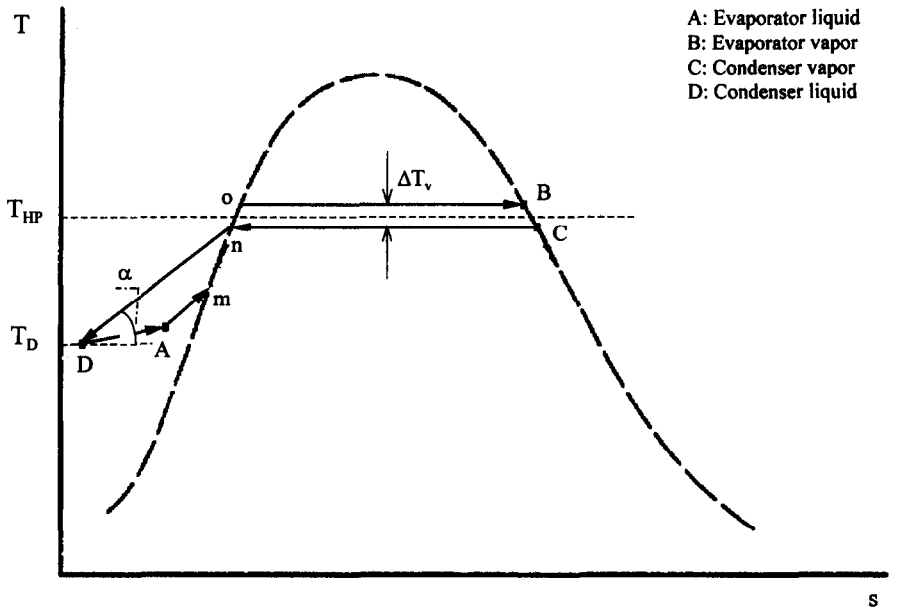

Process	Descriptions
A→B	Heat addition raises both internal energy and pressure of the working fluid.
B→C	Vapor travels from the evaporator to the condenser due to a pressure difference; Entropy increases due to friction.
C→D	Heat rejection at a constant pressure in the condenser
D→A	Liquid travels from the condenser to the evaporator due to a pressure difference; Entropy increases due to friction.

Fig. 3. A T–s diagram of the working fluid circulation in the heat pipe.

B–C and D–A in the adiabatic section has been neglected.

From eqns (10)–(13) the following relation can be obtained:

$$Q_{A-B}+(W_{B-C}+Q_{C-D}+W_{D-A})=0. \quad (14)$$

Equation (14) indicates that the heat addition to the heat pipe system, Q_{A-B}, is not only carried to the condenser but also used to power the "carrier". The power required to pump the working fluid is specified by W_{B-C} and W_{D-A}. The overall energy balance of the heat pipe system suggests that the heat output must be equal to the heat input, i.e. $Q_{out}=Q_{C-D}+W_{B-C}+W_{D-A}$. The frictional work, W_{B-C} and W_{D-A}, is eventually converted into heat dissipation.

The heat pipe operating temperature is usually defined as the vapor temperature. However, as shown in Fig. 3, the vapor temperature changes during process B–C. Since the vapor temperature drop is relatively small, the heat pipe operating temperature, T_{HP}, can be estimated as the arithmetic average of the temperatures at states B and C. Using the "network" method presented earlier in this paper [referring to Fig. 2(b)], the subcooled liquid temperature T_D [T_3 in Fig. 2(b)] and the heat pipe operating temperature T_{HP} [T_{22} or T_{31} in Fig. 2(b)] can be calculated. The four working fluid states, A, B, C and D, can thus be determined by the following procedures:

Step 1. The pressure difference between states B and C can be calculated as [1]

$$\Delta P_{B\to C}=\frac{8Q\mu_v}{\pi\rho_v h_{fg}R_v^4}(0.5L_e+L_a+0.5L_c) \quad (15)$$

where R_v is the radius of the vapor flow channel. If the vapor flow channel is noncircular, an equivalent hydraulic radius must then be used. With ΔP_v known, the vapor temperature difference between states B and C, ΔT_v, can be calculated by using the Clausius–Clapeyron equation by assuming both states B and C are on the saturated vapor line, or by using a thermophysical properties table. Temperatures at states B and C, T_B and T_C, can thus be estimated as

$$T_B=T_{HP}+\tfrac{1}{2}\Delta T_v,\quad T_C=T_{HP}-\tfrac{1}{2}\Delta T_v \quad (16)$$

where T_{HP}, the heat pipe operating temperature, is usually given. States B and C are thus determined by T_B, T_C and the saturated vapor line.

Step 2. State D is determined by P_C (or P_D) and T_D. The condenser liquid temperature, T_D, depends on the condenser cooling condition and is usually a given condition.

Step 3. The liquid pressure difference between states D and A can be calculated as [1]

$$\Delta P_{D\to A} = \frac{\mu_l m_l}{\rho_l A_w K} L_a \tag{17}$$

where A_w is the wick cross-sectional area and K is the wick permeability. The liquid pressure at state A is $P_A = P_D - \Delta P_{D\to A}$.

Another parameter is needed to determine state A. Since no network is done by the system, the area enclosed by the thermodynamic cycle (Fig. 3) must be zero. A careful inspection of Fig. 3 indicates that the area enclosed by AmnDA must equal that enclosed by BCnoB. Based on the assumption of small temperature drops int he vapor and liquid, states A and B are very close to states D and C, respectively, and consequently the following approximate relation can be obtained:

$$|\overline{nD}|\,\Delta s_l \approx \Delta T_v\,\Delta s_{vl} \tag{18}$$

where ΔT_v is the vapor temperature drop during process B–C and $|\overline{nD}|$ is an indication of the liquid subcooling level. From eqn (18), Δs_l can be calculated. Since $\Delta s_l = s_A - s_D$, entropy of the working fluid at state A is found. With P_A and s_A known, state A is thus determined.

There is a more simplified way to determine state A. Since the liquid temperature change in process D–A is small, T_A can be approximated as T_D. With P_A and T_A known, state A is determined.

With states A, B, C and D determined, the working fluid cycle is determined and various parameters including entropy and enthalpy changes, and work done in each process can thus be calculated.

Since Δs_l, ΔT_v and Δs_{vl} are always greater than zero, eqn (18) indicates that $|\overline{nD}| > 0$. Therefore, it can be concluded that the liquid subcooling is a requirement for heat pipe operation. If the condenser cooling capability is inadequate, the thermodynamic cycle shifts upwards to a higher operating temperature to ensure the liquid at state D is in the compressed liquid zone.

Referring to Figs 2(b) and 3, $|\overline{nD}|$ can be approximated as:

$$|\overline{nD}| = \frac{T_C - T_D}{\sin\alpha} = \frac{R_{w,c}Q - 0.5\,\Delta T_v}{\sin\alpha} > 0 \tag{19}$$

where $R_{w,c}$ is the radial condenser wick thermal resistance [R_3 in Fig. 2(b)]. Using eqn (15) and the Clausius–Clapeyron equation, eqn (19) can be rearranged as

$$\frac{\delta}{D}\frac{R_v^4}{L_c(L_e+2L_a+L_c)} > 2k_{eff}\frac{T_{HP}\mu_v}{\rho_v^2 h_{fg}^2} \tag{20}$$

where k_{eff} is the effective thermal conductivity of the liquid-wick structure and can be calculated as:

$$k_{eff} = \frac{k_l[(k_l+k_w)-(1-\varphi)(k_l-k_w)]}{[(k_l+k_w)+(1-\varphi)(k_l-k_w)]}. \tag{21}$$

The left-hand side of eqn (20) is a group of geometric dimensions of the heat pipe which is defined as Φ. The right-hand side is a group of thermophysical properties of the heat pipe working fluid and envelope material which is defined as Θ. Both Φ and Θ have a unit of m^2. Equation (20) can be written as

$$\Psi = \frac{\Phi}{\Theta} > 1. \tag{22}$$

In order to establish the working fluid cycle, the dimensionless number Ψ must be larger than unity, i.e. the magnitude of the geometric dimensions group Φ must be larger than that of the thermophysical properties group Θ. Equation (22) indicates a restraint on the heat pipe geometry under a specific combination of heat pipe working fluid and envelope material. It also provides guidance for selecting an appropriate working fluid and envelope material combination for a specific heat pipe geometry.

It should be noted that eqn (22) has nothing to do with the magnitude of heat transfer rate. No matter how large or small the heat flux is, the heat pipe geometry must be "compatible" with the heat pipe materials. This phenomenon has never been reported in previous studies. A more detailed discussion is presented in the next section.

RESULTS AND DISCUSSIONS

Figure 4 compares the network model with the experimental results from El-Genk and Huang [9]. The water–copper heat pipe's inner and outer diameters are 17.3 and 19.1 mm, respectively. Lengths of the evaporator, adiabatic and condenser sections were 393, 47 and 170 mm, respectively. Two layers of copper screen wick (150 mesh) with a total thickness of 0.3 mm were used. Uniform heat flux heating and convective cooling conditions were applied to the heat pipe. Initially, the heat pipe was in equilibrium with the environment. A uniform heat flux was then applied to the evaporator. After steady state was reached, the heat flux was removed and the heat pipe was cooled until the equilibrium with the environment was reached. During the test the condenser cooling conditions remained unchanged.

The vapor temperature prediction was calculated as T_{22} or T_{31} [referring to Fig. 2(b)]. As shown in Fig. 4, the network model correctly predicted general trends of the heat pipe transients. However, slight overpredictions of the vapor temperature were observed, especially in the early stage of the transient,

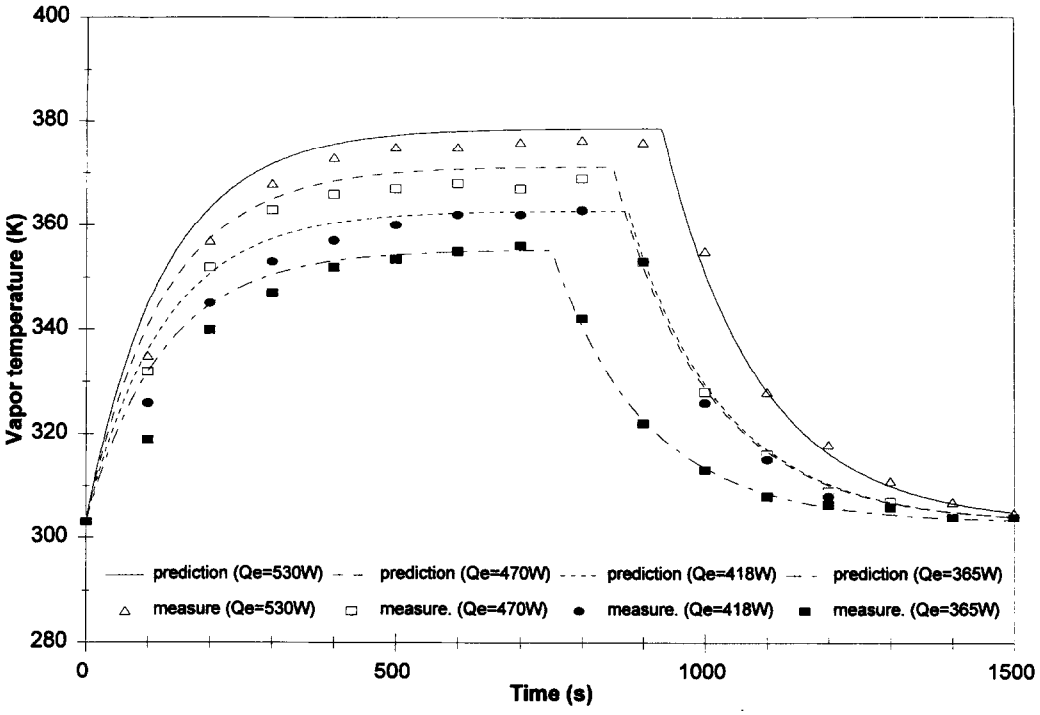

Fig. 4. Comparisons of predicted and measured transient vapor temperatures.

which might be due to the neglecting of heat losses to the environment during the experiments. Additionally, since the model does not include heat capacitance of the test setup including the insulation layers and the cooling-water jacket, the predicted heat pipe transients were slightly faster than those measured. The largest deviation of the predictions from the measurement was less than 5%.

Figure 5 shows comparisons of the network model, a more comprehensive two-dimensional numerical model [10] and a transient lumped model [11]. Geometric dimensions and thermophysical properties of the sodium/stainless heat pipe were: $D_v = 0.014$ m, $L_e = 0.105$ m, $L_a = 0.0525$ m, $L_c = 0.5425$ m, $\delta_{wall} = \delta_{wick} = 0.001$ m, $k_{wall} = 21.7\,W\,m\,K^{-1}$, $k_{eff} = 45$ W m K^{-1}, and $(\rho c_p)_{eff} = 1.05 \times 10^6$ J M^{-3} K^{-1}. The condenser outer surface was exposed to a convective cooling condition with a heat transfer coefficient of 39 $W\,m^{-2}\,K^{-1}$ and an environmental temperature of 300 K. Uniform heat flux heating conditions were applied to the evaporator surface following a specified schedule: at $t = 0$, $Q_e = 623$ W; after $t = 0$, $Q_e = 770$ W.

The vapor temperatures shown as the two-dimensional model predictions were taken as the averages of the vapor temperatures along the heat pipe. As expected, the network model was in excellent agreement with the much more detailed two-dimensional numerical model. For this specific case, the computational time consumed by the network model is about 3 min on a standard 486 PC, compared to 57 min of CPU consumed by the two-dimensional numerical model on a Cray Y-MP8/864 [10]. The comparison in Fig. 5 validated the assumption that the vapor flow has little effect on the transient temperature behavior. The lumped model overpredicted the vapor temperature, which may be due to the neglecting of the interior heat transfer (heat conduction) processes.

Figure 6 illustrates the thermophysical properties group Θ of a mercury–stainless steel heat pipe (assuming the wick porosity $\varphi = 0.7$) at different operating temperatures. Two regions exist which are bounded by the temperature range of the working fluid and separated by the curve of the thermophysical properties group (Θ). If the geometric dimensions group Φ is within region I (above the curve), the working fluid thermodynamic cycle can be successfully established. There is no upper bound to region I. Region II (below the curve) is the area a design engineer should avoid. When the vapor temperature increases, the thermophysical properties group Θ decreases rapidly, providing a larger maneuvering space for the selection of the heat pipe geometric dimensions. Figure 6 can also be used to help select a suitable working fluid and envelope material combination for a given heat pipe geometry.

To illustrate the above discussion, the geometric dimensions group of a simulated mercury–stainless steel heat pipe ($D = 0.02$ m, $\delta_{wall} = 0.0009$ m, $\delta_{wick} = 0.0003$ m, $L_e = 1.6$ m, $L_a = 1.2$ m and $L_c = 0.8$ m) was plotted in Fig. 6. As shown, when the vapor temperature is lower than 300 K, the geometric dimensions group Φ lays below the thermophysical proper-

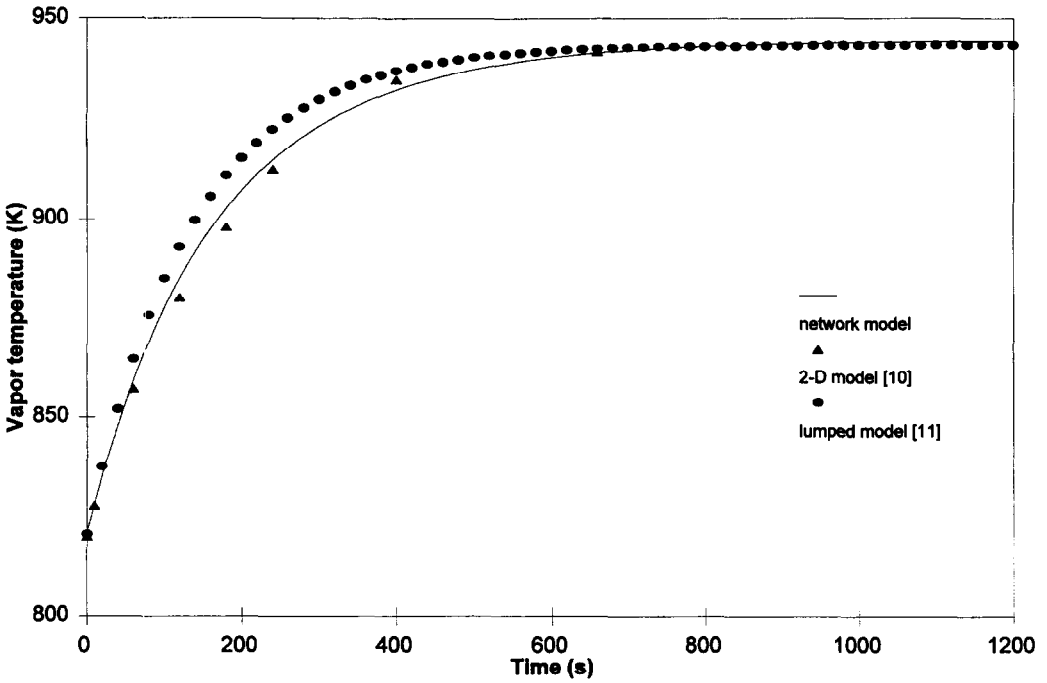

Fig. 5. Comparisons of transient vapor temperatures predicted by the network model, a two-dimensional numerical model and a lumped model.

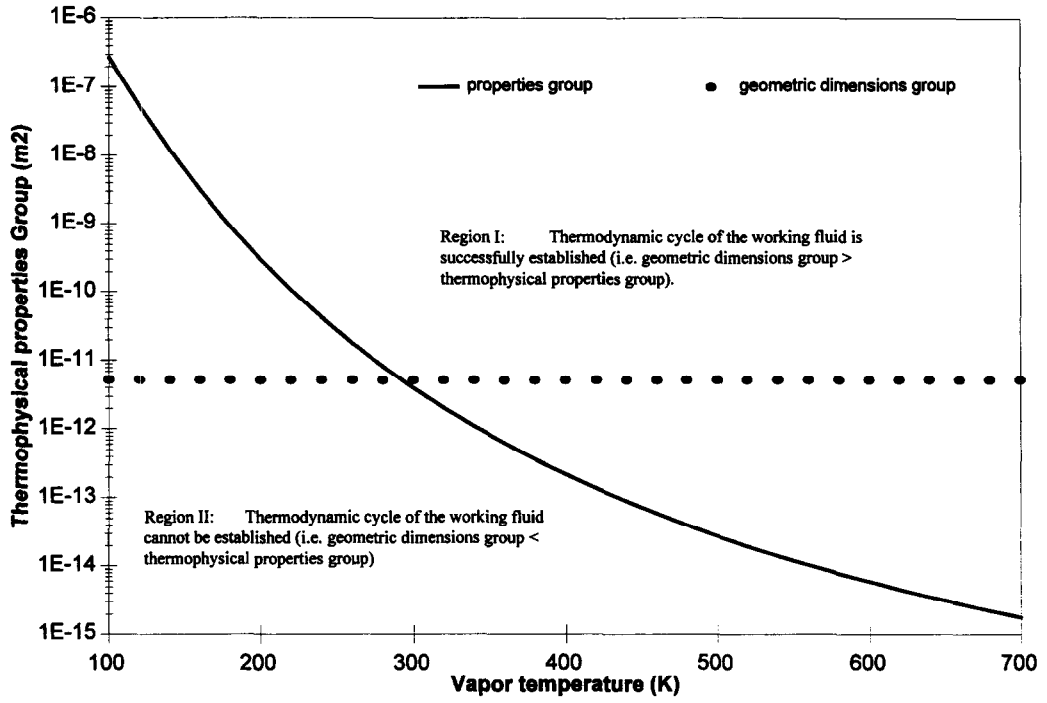

Fig. 6. Thermophysical properties group of a mercury–stainless steel heat pipe.

ties group Θ, indicating that the heat pipe, with the specified dimensions, cannot operate properly. Once the temperature passes the critical 300 K, the requirement for a successful thermodynamic cycle (i.e. $\Phi > \Theta$) is satisfied and the heat pipe starts functioning. The requirement that a heat pipe must reach a minimum operating temperature before any significant heat transfer can be detected is a phenomenon

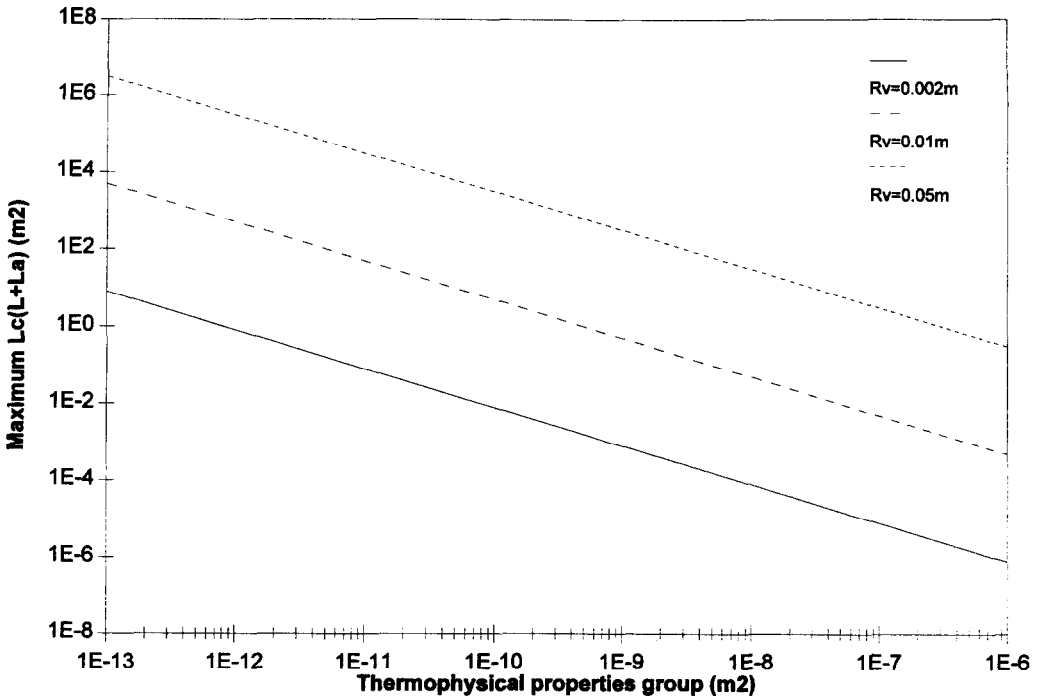

Fig. 7. Maximum heat pipe length limited by thermodynamic requirement.

that has been observed in previous experiments [4].

It must be pointed out that the minimum operating temperature mentioned above is different from the melting temperature of the working fluid. This minimum operating temperature is directly related to the establishment of the critical working fluid cycle inside a specific heat pipe. If the heat pipe is designed longer or smaller, corresponding to a smaller value of the geometric dimensions group Φ, the minimum operating temperature would be higher. As shown in Fig. 6, a mercury–stainless steel heat pipe with a geometric dimensions group less than 2×10^{-15} m^2 can never function properly no matter what heating and cooling conditions are applied. Therefore, there exists a limitation to the heat pipe diameter or length.

Figure 7 shows the maximum heat pipe length restricted by the thermophysical properties group Θ of the heat pipe working fluid and envelope material combination. The wick thickness to pipe diameter ratio was assumed 0.05 for all curves. On logarithmic scales, linear relations between the maximum $L_c(L+L_a)$ and the value of Φ was observed for the fixed vapor channel radius.

As shown, a heat pipe with a larger thermophysical properties group (Θ) has a smaller maximum length (i.e. shorter maximum heat transport distance). Therefore, in order to transport heat through a longer distance, a working fluid with a larger latent heat of vaporization, a smaller vapor viscosity and a larger vapor density (or higher vapor pressure) is preferred. It is interesting to point out that the concept of the thermophysical properties group Θ proposed in this paper is somewhat similar to the working fluid merit number defined as $\sigma_l L\rho_l/\mu_l$ by Dunn and Reay [5]. However, unlike the merit number, the thermophysical properties group Θ should be as small as possible. Additionally, the thermophysical properties group Θ was derived from the First Law of Thermodynamics and thus has clear physical meaning.

Figure 8 shows thermophysical properties of various working fluid and envelope material combinations (assuming the wick porosity $\varphi = 0.5$ for all cases). In cryogenic temperature range (4–200 K), two combinations, helium–SST (stainless steel) and nitrogen–SST were illustrated. Both working fluids have relatively narrow temperature range and correspondingly steep change in magnitude of the thermophysical properties group Θ. Both helium–SST and nitrogen–SST have thermophysical properties groups below 10^{-13} m^2. Therefore, if a helium–SST or nitrogen–SST heat pipe has a vapor channel diameter of 4 mm and a wick thickness of 0.2 mm, its maximum length $L_c(L+L_a)$ is approximately 10 m^2 (see Figure 7).

In the temperature range of 200–500 K, ethane–SST, ammonia–SST, Freon–SST, acetone–SST and ethanol–SST were illustrated. As shown, the combination of ammonia–SST corresponds to the smallest magnitude of the thermophysical properties group (Θ) for most of the temperature range. The combination of Freon-11 and stainless steel has a large value of Θ ($\sim10^{-10}$ m^2) at lower temperatures, presenting some restrictions to the heat pipe dimensions.

Mercury–SST combination has a wide temperature range from 100 K to nearly 700 K. However, at tem-

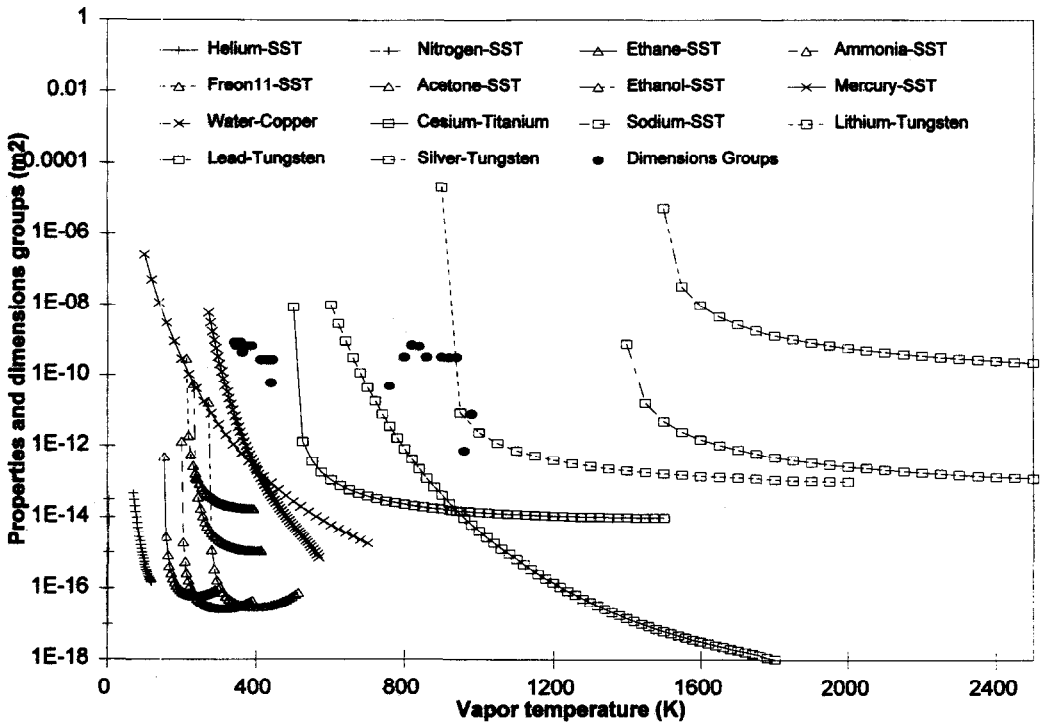

Fig. 8. Thermophysical properties groups of various material and fluid combinations.

peratures less than 200 K the magnitude of the thermophysical properties group (Θ) is above 10^{-10} m^2, indicating that small-diameter/long heat pipes may not function properly in that temperature range. Water–copper combination exhibits similar trends to mercury–SST.

For high-temperature applications, cesium–titanium, sodium–stainless steel, lithium–tungsten, lead–tungsten and silver–tungsten were illustrated. The combination of sodium–SST is the most desirable because of its exceptionally small magnitude of Θ over a wide temperature range of 700–1800 K. On the other hand, the smallest Θ of the silver–tungsten combination is approximately 10^{-9} m^{-2}. Referring to Fig. 7, the maximum length $L_c(L+L_a)$ is only 1 m^2 for a typical silver–tungsten heat pipe with a vapor channel diameter of 20 mm and a wick thickness of 1 mm. Assuming that $L_e = L_a = L_c$, the maximum total length of the silver–tungsten heat pipe is 0.85 m. It is indeed very surprising that the combination of working fluid and envelope material has such a rigid restriction of the heat pipe geometric dimensions.

Geometric dimensions groups of heat pipes investigated by previous researchers [6, 7, 9–17] were also plotted in Fig. 8. These heat pipes include three combinations: water–copper, mercury–SST and sodium–SST. In all cases, the thermodynamic requirement that Φ must be larger than Θ was satisfied.

It should be emphasized that, for most applications, the thermodynamic requirement can easily be satisfied. However, attention must be paid to special cases involving working fluid-envelope material combinations with large magnitudes of Θ (such as silver–tungsten) or having small/long geometry requirement.

CONCLUSIONS

The heat pipe is a network system consisting of a number of thermal components, whose transient behavior can be analyzed by classical system analysis theories. Governing equations of the transient heat pipe behavior can be simplified into a set of first-order linear ordinary differential equations. The Runge–Kutta method can be used to obtain transient heat pipe temperatures. Comparisons with previous experimental and numerical results validated the network model.

In order to establish a continuous heat transfer process, the working fluid must continuously circulate inside the heat pipe. The internal temperature/pressure difference is essential to the working fluid circulation. A portion of the thermal energy (heat) added into the heat pipe is used to pump the working fluid. Successful establishment of the thermodynamic cycle requires "compatibility" between thermophysical properties of the working fluid-envelope material combination and geometric dimensions of the heat pipe. If this requirement (dimensionless number $\Psi = \Phi/\Theta > 1$) is not satisfied, the heat pipe cannot function properly.

The analysis presented in this paper provides a reasonably accurate and practically simple way to transient heat pipe analysis and heat pipe design.

REFERENCES

1. Faghri, A., *Heat Pipe Science and Technology*, Taylor & Francis, Washington, DC, 1995.
2. Colwell, G. T. and Modlin, J. M., Mathematical heat pipe models. *Proceedings of the 8th International Heat Pipe Conference*, Vol. 1, Beijing, 1992.
3. Vasiliev, L. L. and Konev, S. V., Thermodynamic analysis of heat pipe operation. *Proceedings of the 4th International Heat Pipe Conference*, London, 1981.
4. Richter, R. and Gottschlich, J. M., Thermodynamic aspects of heat pipe operation. *Journal of Thermophysics and Heat Transfer*, 1994, **8**(2), 334–340.
5. Dunn, P. D. and Reay, D. A., *Heat Pipes*, 4th edn. Pergamon, Oxford, 1994.
6. Bowman, W. J., Numerical modeling of heat-pipe transients. *Journal of Thermophysics and Heat Transfer*, 1991, **5**(3), 374–379.
7. Bowman, W. J., Winn, R. C. and Martin, H. L., Transient heat-pipe modeling: a quasi-steady, incompressible vapor model. *Journal of Thermophysics and Heat Transfer*, 1992, **6**(3), 571–574.
8. Zuo, Z. J., Faghri, A. and Langston, L., Numerical analysis of heat pipe turbine vane cooling. *Journal of Turbomachinery*, 1997 (in press).
9. El-Genk, M. S. and Huang, L., An experimental investigation of the transient response of a water heat pipe. *International Journal of Heat and Mass Transfer*, 1993, **36**(15), 3823–3830.
10. Cao, Y. and Faghri, A., Transient two-dimensional compressible analysis for high-temperature heat pipes with pulsed heat input. *Numerical Heat Transfer, Part A*, 1990, **18**, 483–502.
11. Faghri, A. and Harley, C., Transient lumped heat pipe analysis. *Heat Recovery Systems and CHP*, 1994, **14**(4), 351–363.
12. Cao, Y. and Faghri, A., Transient multidimensional analysis of nonconventional heat pipes with uniform and nonuniform heat distributions. *Journal of Heat Transfer*, 1991, **113**, 995–1002.
13. Chen, M. and Faghri, A., An analysis of the vapor flow and the heat conduction through the liquid-wick and pipe wall in a heat pipe with single or multiple heat sources. *International Journal of Heat and Mass Transfer*, 1990, **33**(9), 1945–1955.
14. Gernert, N. J., Analysis and performance evaluation of heat pipes with multiple heat sources. *AIAA/ASME 4th Joint Thermophysics and Heat Transfer Conference*, 1986.
15. Faghri, A. and Buchko, M. T., Experimental and numerical analysis of low-temperature heat pipes with multiple heat sources. *Journal of Heat Transfer*, 1991, **113**, 728–734.
16. Ivanovskii, M. N., Sorokin, V. P. and Yagodkin, I. V., *The Physical Principles of Heat Pipes*. Oxford University Press, Oxford, 1982.
17. Kemme, J. E., Ultimate heat pipe performance. *IEEE Transactions on Electronic Devices*, 1969, **ED16**, 717–723.